

Ferromagnetic Impurity Induced Majorana Zero Mode in Iron-Based Superconductor

Rui Song,^{1,2,3} Ping Zhang,^{4,2,5,*} Xian-Tu He,^{2,5} and Ning Hao^{3,†}

¹HEDPS, Center for Applied Physics and Technology and School of Physics, Peking University, Beijing 100871, China

²HEDPS, Center for Applied Physics and Technology and School of Engineering, Peking University, Beijing 100871, China

³Anhui Key Laboratory of Condensed Matter Physics at Extreme Conditions,
High Magnetic Field Laboratory, HFIPS, Anhui, Chinese Academy of Sciences,
and University of Science and Technology of China, Hefei, China

⁴School of Physics and Physical Engineering, Qufu Normal University, Qufu 273165, China

⁵Institute of Applied Physics and Computational Mathematics, Beijing 100088, China

Recent experiments reported the puzzling zero energy modes associated with ferromagnetic impurities in some iron-based superconductors with topological band structures. Here, we show that the sufficiently strong exchange coupling between a ferromagnetic impurity and substrate can trigger a quantum phase transition, beyond which, the phase of the topological surface superconducting order parameter around the impurity acquires a sign-change. In such a case, we prove that a Kramers degenerate pair of Majorana modes can be induced at the boundary separating the two sign-change regimes and trapped around the impurity in the topological surface superconducting state. Furthermore, we show that our theory can explain the controversial observations and confusing features of the zero energy modes from recent experiments in some iron-based superconductors.

In superconductor, the impurity can induce various quasi-particle states, such as Yu-Shiba-Rusinov (YSR) state from the classical impurity scattering potential[1–3] and Kondo resonance state from the impurity in quantum limit[4]. Through elucidating their properties, one can obtain much critical information on electron pairing[5]. Meanwhile, the quasi-particle state itself can manifest some unexpected behaviors. In particular, a interstitial iron impurity (IFI) induced robust zero-energy mode (ZM) has been reported by the scanning tunnelling microscopy/spectroscopy (STM/S) in iron-based superconductor Fe(Te,Se)[6]. The subsequent studies have been extended to other iron-based superconductors such as monolayer Fe(Te,Se)/SrTiO₃ and LiFeAs, and the similar ZM is also observed[7, 8]. Experimentally, the ZM can only be observed on partial iron impurities and is robust against the external magnetic field, and the critical temperature is much below the superconducting transition temperature T_c . Besides, these materials share a remarkable feature of possessing topological bands, which implies the ZMs could be Majorana modes. On the contrary, some revisited studies on Fe(Te,Se) claim the observed ZM is just trivial YSR states with near-zero-energy electron-like and hole-like components[9, 10]. Thus, the understandings of the properties and the mechanism of the ZMs in these iron-based superconductors are still in debate[6–10].

In this work, we first perform the first-principles calculations to investigate the interaction between IFI and substrate FeSe_{0.45}Te_{0.55}. The numerical results indicate the exchange coupling $J(\mathbf{r}, z)$ between magnetic moment of IFI and spin of the $3d$ electron of FeSe_{0.45}Te_{0.55} has the form of Friedel-like oscillation with the characteristic length a_0 of lattice constant of iron square lattice. The amplitude of $J(\mathbf{r}, z)$ and the magnetic moment of IFI strongly depend on the height z between IFI and sub-

strate. We further consider the impact of IFI on topological surface superconducting order parameter $\Delta(\mathbf{r})$ by solving the Bogoliubov–de Gennes (BdG) equations defined on iron square lattice with self-consistency. We find that there exists a quantum phase transition (QPT) at a critical height z_c , *i.e.* a critical $J_c(\mathbf{r}, z_c)$, beyond which, $\Delta(\mathbf{r})$ change sign in the $r < a_0$ regime. Then, we prove that a Kramers degenerate pair of Majorana ZMs can be induced at the boundary separating the two sign-change regimes and trapped by the IFI. For the smaller $J(\mathbf{r}, z) < J_c(\mathbf{r}, z_c)$, the QPT cannot be triggered. The IFI can only induce the trivial YSR states, which has the near-zero energy in vicinity of QPT. Within this picture, the contradictions between the results from different STM/S measurements can be solved, and properties of the ZMs, such as robustness against external magnetic field and lower critical temperature can also be understood.

The STM experiment shows that the height of IFI can be tuned by STM tip[8, 10]. During the process of approaching, transition from YSR states to ZMs happens[8]. It indicates that the coupling between IFI and substrate play a crucial role to observe ZMs. To elucidate properties of such coupling, we construct a $9 \times 9 \times 1$ supercell including substrate Fe(Te,Se) with a suspended IFI. Here, we only summarize main results in Fig. 1, with calculation details in Ref. [11]. From Fig. 1 (a), there exists a strong charge transfer between IFI and substrate iron atoms, and such transfer decays abruptly as expected. The calculated spin polarizations of substrate shown in Fig. 1 (b) indicate $J(\mathbf{r}, z_0)$ has the form of Friedel-like oscillation, which is consistent with the neutron scattering experiment on the Fe(Te,Se) with higher concentration of Te[12]. The characteristic length measured oscillation period is about lattice constant a_0 from Fig. 1 (b). The findings are further supported by mag-

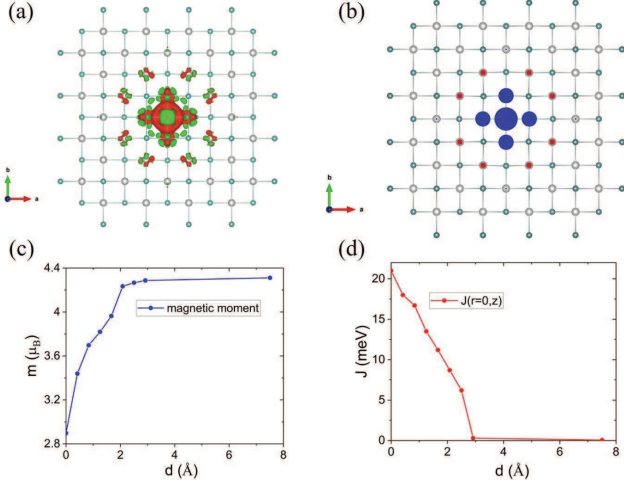


FIG. 1: (a) The spatial distributions of differential charge density of a supercell involving a $9 \times 9 \times 1$ Fe(Te,Se) substrate and a suspended IFI. (b) The spatial distributions of the induced spin polarizations of the 3d electrons of iron atoms in the substrate. The size and color of the dots denote the strength and direction of the spin polarization, respectively. (c)-(d) The magnetic moment of IFI and the effective exchange coupling $J(r=0, z)$ as a function of the height d between the IFI and the substrate, respectively.

netic moment of IFI as a function of height, as shown in Fig. 1 (c). As IFI approaches the substrate, the magnetic moment of IFI is suppressed. It indicates spin transfer also happens and exchange coupling between magnetic moment of IFI and substrate is strong. The strength of $J(\mathbf{r}=0, z_0)$ can be roughly estimated and is shown in Fig. 1 (d)[11].

Another crucial experimental signature is the presence of a level crossing at the transition from YSR states to ZMs, and the level crossing is robust against magnetic field[8]. This signature indicates the suitable model related to STS experiments is topological surface Dirac bands with trivial s-wave pairing[11]. Thus, we start with such a model defined on square lattices to evaluate impact of IFI to $\Delta(\mathbf{r})$ of topological Dirac states on the surface of Fe(Te,Se) substrate. The model Hamiltonian is,

$$H_{eff} = H_{BdG} + H_{coup}, \quad (1)$$

and

$$H_{BdG} = -\mu \sum_i c_i^\dagger c_i - it \sum_{\langle i,j \rangle} c_{i\sigma}^\dagger (\mathbf{S}^{\sigma\sigma'} \times \hat{\mathbf{d}}_{ij}) \cdot \hat{\mathbf{z}} c_{j\sigma'} + \sum_i \Delta_i (c_{i\uparrow}^\dagger c_{i\downarrow}^\dagger + c.c.), \quad (2)$$

$$H_{coup} = \int d\mathbf{r} J(\mathbf{r}, z_0) \mathbf{S}_{imp} \cdot \boldsymbol{\sigma}. \quad (3)$$

Here, μ is the chemical potential. The second term in Eq. (2) describes the topological surface Dirac states defined

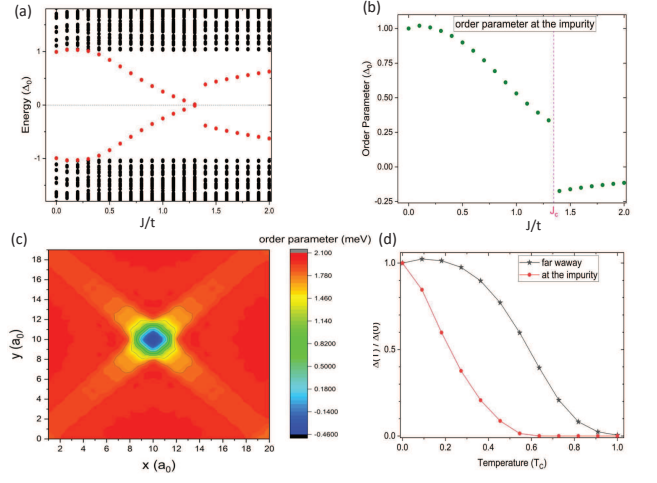


FIG. 2: (a) The energy spectrum as a function of $J(r=0, z)$ from the self-consistent solution of Eq. (1). The red dots with opposite energy are a pair of YSR states. (b) The order parameter of superconducting state $\Delta(r=0)$ as a function of $J(r=0, z)$ from the self-consistent solution of Eq. (1). (c) The spatial distributions of $\Delta(r)$ under the condition $J(r=0, z) = 1.5t$. (d) The temperature evolution of the $\Delta(r)$ from the self-consistent solution of Eq. (1).

on square lattices. $\hat{\mathbf{d}}_{ij}$ is the unit vector pointing from i to j . Δ_i is site-dependent superconducting order parameter. Note that such trivial s-wave pairing is good approximation for the topological surface Dirac state, can give the consistent results with the STS experiments[8, 11], and is widely adopted to study the topological properties of the ion-based superconductors[13–22]. \mathbf{S}_{imp} and $\boldsymbol{\sigma}$ in Eq. (3) label magnetic moment of IFI and spin of Fe of substrate, respectively. Here, we only consider z -directional spin polarization. $J(\mathbf{r}, z_0)$ is important only in the first oscillating period a_0 . The nearest-neighbor $J(\mathbf{r}, z_0)$ is less than J_c according to the calculation. Here, we only consider the on-site term $J(\mathbf{r}=0, z_0)$ for simplicity[11]. As $J(\mathbf{r}=0, z_0)$ increases from zero, there exists a QPT[5, 23, 24] at a critical $J_c \sim 1.3t$, beyond which, $\Delta(r)$ suddenly changes sign and becomes negative, as shown in Fig. 2 (b). Meanwhile, the level crossing of two components of YSR states happens, as shown in Fig. 2 (a). Then, the spacial distributions of $\Delta(r)$ in Fig. 2 (c) indicate $\Delta(r)$ acquires a π phase difference in $r < R_0$ regime in comparison with that in $r > R_0$ regime. Note that R_0 can take the value of lattice constant a_0 if the nearest-neighbor term of $J(\mathbf{r}, z_0)$ is involved[11]. This is a very crucial result from the effect of IFI[23–27]. Though QPT is not driven by temperature, increase of temperature could quench it. Thereafter, we calculates the critical temperature T_q of QPT and find T_q is quite lower than bulk superconducting transition temperature T_c . We will return to this temperature effect below.

Now, we consider the effect of spacial variation of $\Delta(r)$ to topological surface states. The effective Hamiltonian describing the topological surface superconductivity with sign-change boundary condition is,

$$H_s = [v_F(\mathbf{k} \times \boldsymbol{\sigma}) \cdot \hat{\mathbf{z}} - \mu]\tau_z + \Delta(r)\tau_x. \quad (4)$$

Here, H_s is spanned in Nambu space, *i.e.*, $[c_\uparrow, c_\downarrow, c_\downarrow^\dagger, -c_\uparrow^\dagger]$. $\tau_{x/z}$ is Pauli matrix to span particle-hole space. $\Delta(r) = -\Delta_1$ when $r < R_0$ and $\Delta(r) = \Delta_2$ when $r > R_0$ with $\Delta_{1/2} > 0$ and $\Delta_1 < \Delta_2$. The phase of $\Delta_{1/2}$ is uniform and is omitted due to the absence of topological defect such as vortex. Thus, $\Delta_{1/2}$ is angle-independent and $\Delta(r)$ is real in Eq. (4). In continuum limit, eigen-equation of H_s is

$$H_s(\mathbf{k} \rightarrow -i\nabla)\psi(r, \theta) = E\psi(r, \theta), \quad (5)$$

which can be solved under boundary conditions with a $0 - \pi$ disk junction shown in Fig. 3 (c).

Before solving equation (5), we give a simple physical picture to understand existence of a Kramers degenerate pair of Majorana ZMs of the model. The Hamiltonian in Eq. (4) preserves particle-hole symmetry (PHS) with $\mathcal{C} = i\sigma_y\tau_yK$ and time-reversal symmetry (TRS) with $\mathcal{T} = i\sigma_y\tau_0K$. The $0 - \pi$ disk junction in Fig. 3 (c) can come from the combo of geometries in Figs. 3 (a) and (b). We know that both geometries in Figs. 3 (a) and (b) host none edge bound states due to Dirac cone itself being two-dimensional boundary states[11]. However, when two geometries in Figs. 3 (a) and (b) are combined to form $0 - \pi$ disk junction in Fig. 3 (c), edge bound states must emerge. This behavior can be understood from Fig. 3 (d) to (e). $0 - \pi$ disk junction in Fig. 3 (e) can also be obtained by bending $0 - \pi$ line junction in Fig. 3 (d) to connect two ends. It is well known that $0 - \pi$ line junction can support the one-dimensional linear-dispersion bound states[28, 29]. Likewise, $0 - \pi$ disk junction in Figs. 3 (c) and (e) should also have edge bound states. Such difference between Figs. 3 (a) and (b) and Figs. 3 (c) and (e) lies in that the wave function $\psi(r, \theta)$ in $0 - \pi$ disk junction in Figs. 3 (c) and (e) must obey crucial *antiperiodic boundary condition*, *i.e.*, $\psi(r, \theta) = -\psi(r, \theta + 2\pi)$ to get bound states, which is explicitly pointed out by Fu *et al*[28]. Further considering geometry changes from Fig. 3 (d) to (e), the one-dimensional linear-dispersion bound states have to split into series quantized modes labeled by quantum numbers of angular momentum, among which, a pair of Majorana ZMs, must emerge. Such emergence can be understood from vortex case shown in Fig. 3 (f). The single-value condition requires wave function in vortex case is *periodic*, *i.e.*, $\psi_v(r, \theta) = \psi_v(r, \theta + 2\pi)$. If one does a gauge transformation $\psi_v(r, \theta) \rightarrow e^{i\sigma_z\theta/2}\psi'_v(r, \theta)$, the phase winding of superconducting pair is eliminated, and new wave function $\psi'_v(r, \theta)$ must obey *antiperiodic boundary condition*

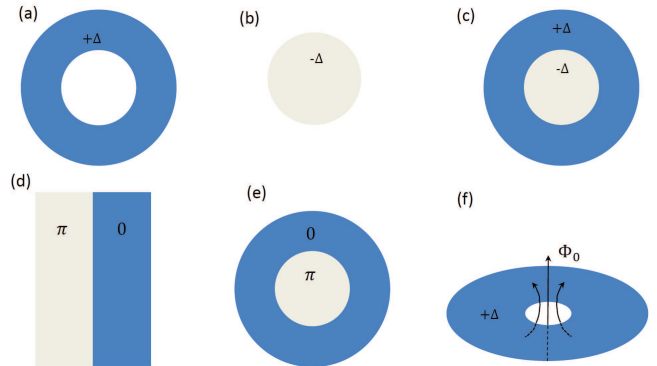


FIG. 3: (a) The infinite ring with uniform positive superconducting pairing Δ . (b) The finite disk with uniform negative superconducting pairing $-\Delta$. (c) Our $0 - \pi$ disk junction is the spacial combo of (a) and (b). (d)-(e) The schematic plotting to show the $0 - \pi$ line junction bends to form a $0 - \pi$ disk junction as same as (c). (f) The infinite disk with uniform positive superconducting pairing Δ , which has a centric hole with a superconducting flux quanta.

$\psi'_v(r, \theta) = -\psi'_v(r, \theta + 2\pi)$ [11]. It means that applying magnetic flux is equivalent to changing boundary conditions of wave function[30]. In this sense, our case is equivalent to vortex case by further taking into account another TR counterpart[11]. Therefore, Majorana ZMs must emerge for Hamiltonian in Eq. (4) with $0 - \pi$ disk junction in Figs. 3 (c) and (e)[31].

The above arguments can be exactly proven by both analytic and numerical solutions of Eq. (5)[11]. For boundless $0 - \pi$ disk junction in Fig. 3 (c), wave function of the first Majorana ZM takes the form $\psi_1(r, \theta) = [e^{-i\theta/2}u_\uparrow(r), e^{i\theta/2}u_\downarrow(r), e^{-i\theta/2}v_\downarrow(r), -e^{i\theta/2}v_\uparrow(r)]$ with condition $u_\sigma(r) = -v_\sigma(r)$. $u_\sigma(r) = a_\sigma J_{\mp 1/2}(k_F r)e^{r/\xi_1}$ for $r < R_0$ and $u_\sigma(r) = b_\sigma J_{\mp 1/2}(k_F r)e^{-r/\xi_2}$ for $r > R_0$. $J_{\mp 1/2}(k_F r)$ is Bessel functions with $\mp 1/2$ for spin up and down, respectively. a_σ and b_σ are coefficients determined by continuity and normalization of wave function. Fermi wave vector $k_F = \mu/v_F$. Decay length $\xi_{1/2} = v_F/\Delta_{1/2}$. The wave function of the second Majorana ZM can be obtained by $\psi_2(r, \theta) = \mathcal{T}\psi_1(r, \theta)$. Note that the minigap to protect Majorana ZMs is proportional to v_F/R_0 , which ensures only a pair of Majorana ZMs survive for small R_0 [11]. STS measured differential conductance $dI/dV \propto \sum_\sigma r[|u_\sigma(r)|^2\delta(\omega - eV) + |v_\sigma(r)|^2\delta(\omega + eV)]$. The case for Majorana ZMs is plotted in Fig. 4 (b), from which, spacial profile of dI/dV is consistent with observations in monolayer Fe(Te,Se)/SrTiO₃[7] but has subtle difference near $r = 0$ in comparison with the measurements in bulk Fe(Te,Se) and LiFeAs[6, 8]. We argue this tiny difference is from effect of IFI, such as mixture of electronic state, electron's inelastic tunneling process or finite quasi-particle scattering etc. In Fig. 4 (c), we consider modulation from finite quasi-particle

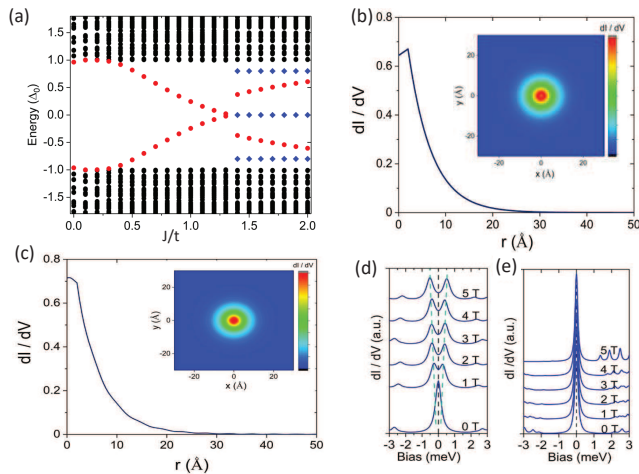


FIG. 4: (a) The overall energy spectrum from both YSR states (red color) of IFI scattering and the Majorana ZMs (blue color at zero energy) at the boundary separated the sign-change regimes as a function of $J(r=0, z)$. The former is the same as Fig. 2 (a), and the latter is from the numerical solution of Eq. (4) defined in the finite disk configuration. (b) The simulated dI/dV profile for the Majorana zero mode from the analytic solutions of Eq. (4) defined in the boundless disk configuration. (c) The simulated dI/dV profile for the Majorana ZMs by take into account the quasi-particle scattering. The inset in (b) and (c) are the simulated dI/dV two-dimensional spacial profiles. (d) and (e) The external magnetic field effect to the YSR states and the Majorana ZMs, respectively.

scattering and resulting spectrum is quite similar to cases in bulk Fe(Te,Se) and LiFeAs[11]. For finite $0 - \pi$ disk junction, numerical results are also consistent with analytic solutions[11].

Aforementioned theory can be utilized to understand multiple features and common properties of ZMs in iron-based superconductors. We summarize bound-state spectrum as function as $J(\mathbf{r}=0, z_0)$ in Fig. 4 (a). There exists a pair of near-zero-energy YSR states from IFI when $J(\mathbf{r}=0, z_0)$ is close to J_c . The electron-like and hole-like components of a pair of near-zero-energy YSR states has opposite spin polarizations. Thus, the whole of them shows no spin-resolved feature. When $J(\mathbf{r}=0, z_0)$ is larger than J_c , a pair of near-zero-energy YSR states steeply split, and the robust Majorana ZMs emerge and located at the boundary separated by two sign-change regimes. Note that the boundary is very close to the IFI. Thus, the contradictions from different STM/S experiments root in the selected IFIs with different exchange couplings $J(\mathbf{r}=0, z)$, which coincides with the fact that ZMs can be only observed on a partial IFIs[6–8]. The fragileness of near-zero-energy YSR state and the robustness of Majorana ZMs against external magnetic field can also be understood. Consider Zeeman energy m_z of ex-

ternal magnetic field, for a pair of near-zero-energy YSR states, opposite spin polarization indicates they have to split according to $m_z\sigma_z$, as shown in Fig. 4 (d). For Majorana ZMs, the Hamiltonian $H_s(\mathbf{k} \rightarrow -i\nabla)$ defined in $0 - \pi$ disk junction possesses a hidden mirror symmetry $\mathcal{M}_{l=0} = i\sigma_y\tau_y\hat{O}(r)$. $\hat{O}(r)$ is a spacial inverse operator along radial direction with inverse center at R_0 [11]. The degeneracy of a pair of Majorana ZMs is protected by this hidden mirror symmetry against σ_z and σ_x Zeeman field. However, in-plane Zeeman term $m_y\sigma_y$ can split the degeneracy of Majorana ZMs[33]. This behavior can be testified by future experimental measurement. Turn to band structure, Zeeman term m_z can be added into H_s in Eq. (4) to open a gap to Dirac bands. Then, the solution forms of Majorana ZMs are not changed but with a modulated $k'_F = \sqrt{\mu^2 - m_z^2}/v_F$ [11]. Thus, the Majorana ZMs are robust under condition $m_z < \mu$, as shown in Fig. 4 (e). Note that H_s plus $m_z\sigma_z$ is also one copy of decoupled Hamiltonian to describe the case in monolayer Fe(Te,Se)/SrTiO₃[7], in which, Dirac bands are from the bulk. Some experiments have observed that Majorana ZMs disappear at a temperature below T_c [6–8]. This behavior can also be understood from the self-consistent calculation results in Fig. 2 (d). The sign-change $\Delta(r=0)$ decays to zero at about $T_q \sim 0.6T_c$. We argue this is the primary reason for temperature effect in spite of the possible quasi-particle poisoning[18, 32]. It is worth noting that magnetic impurity induced robust energy mode has also been observed in PbTaSe₂[34], which also has topological bands and is superconducting. Within our theory, the observations in PbTaSe₂ can be well understood.

At last, the reliability of theory can be enhanced by estimating some relevant parameters. The first one is $J_c \sim 1.3t$ with t measuring the energy scale of the surface Dirac state, *i.e.*, $t \sim v_F k_F$. According to the experiment[18, 35], $v_F \sim 250\text{meV}\text{\AA}$, and $k_F \sim 0.02\text{\AA}^{-1}$. Then, $J_c \sim 7\text{meV}$. It is also the reason why single IFI with quite small exchange coupling can induce the QPT and relevant Majorana modes. IFI can have a magnetic moment $m \sim 5\mu_B$, which induces a magnetic dipole field $B(r) = \mu_0 m / 4\pi r^3$ [36, 37]. The induced magnetic flux can be calculated by setting lower limit of integral cutoff to be a Wigner-Seitz radius of square lattice. If one quantized magnetic vortex emerges, it require the magnetic moment extend to be $10^4\mu_B$, which is only possible for a magnetic cluster in nanoscale.

In conclusion, we provide a new understanding to resolve the debate about whether STM/S observed ZMs induced by IFI on some iron-based superconductors is Majorana ZMs or not. We find a QPT can be triggered by the exchange coupling between the IFI and substrate. Then, the local superconducting order parameter of the surface superconducting state changes sign around the impurity, and we prove that a robust Kramers degenerate pair of Majorana ZMs can be induced and trapped

around the IFI. Our theory can explain series confusing features observed by experiments. More meaningfully, our theory can be extended to other material categories, which host both topological bands and superconductivity.

The authors thank J. P. Hu, Z. Fang, C. Fang, X. X. Wu, S. B. Zhang, S. S. Qin, F. W. Zheng, H. F. Du, L. Shan, Z. Y. Wang, S. C. Yan and X. Y. Hou for helpful discussions. This work was financially supported by the National Key R&D Program of China No. 2017YFA0303201, National Natural Science Foundation of China under Grants (No. 12022413, No. 11674331, No.11625415), the ‘‘Strategic Priority Research Program (B)’’ of the Chinese Academy of Sciences, Grant No. XDB33030100, the ‘100 Talents Project’ of the Chinese Academy of Sciences, the Collaborative Innovation Program of Hefei Science Center, CAS (Grants No. 2020HSC-CIP002), the CASHIPS Director’s Fund (BJPY2019B03), the Science Challenge Project under Grant No. TZ2016001, the Major Basic Program of Natural Science Foundation of Shandong Province (Grant No. ZR2021ZD01). A portion of this work was supported by the High Magnetic Field Laboratory of Anhui Province, China.

* Electronic address: zhang’ping@iapcm.ac.cn

† Electronic address: haon@hmf.ac.cn

- [1] L. Yu, Bound state in superconductors with paramagnetic impurities, *Acta Phys. Sin.* **21**, 75–91 (1965).
- [2] H. Shiba, Classical spins in superconductors. *Prog. Theor. Phys.* **40**, 435–451 (1968).
- [3] A. I. Rusinov and P. M. Z. E. T. Fiz, On the theory of gapless superconductivity in alloys containing paramagnetic impurities, *JETP Lett.* **9**, 1101–1106 (1968).
- [4] J. Kondo, Resistance minimum in dilute magnetic alloys, *Prog. Theor. Phys.* **32**, 37 (1964).
- [5] A. V. Balatsky, I. Vekhter, and Jian-Xin Zhu, Impurity-induced states in conventional and unconventional superconductors, *Re. Mod. Phys.* **78**, 373-433 (2006).
- [6] J-X. Yin, Z. Wu, J-H. Wang, Z.-Y. Ye, J. Gong, X.-Y. Hou, L. Shan, A. Li, X.-J. Liang, X.-X. Wu, J. Li, C.-S. Ting, Z.-Q. Wang, J.-P. Hu, P.-H. Hor, H. Ding and S. H. Pan, Observation of a robust zero-energy bound state in iron-based superconductor Fe(Te,Se), *Nat. Phys.* **11**, 543 (2015)
- [7] C. Liu, C. Chen, X. Liu, Z. Wang, Y. Liu, S. Ye, Z. Wang, J. Hu and Jian Wang, Zero-energy bound states in the high-temperature superconductors at the two-dimensional limit, *Sci. Adv.* **6**, eaax7547 (2020)
- [8] P. Fan, F. Yang, G. Qian, H. Chen, Y.-Y. Zhang, G. Li, Z. Huang, Y. Xing, L. Kong, W. Liu, K. Jiang, C. Shen, S. Du, J. Schneeloch, R. Zhong, G. Gu, Z. Wang, H. Ding and H.-J. Gao, Observation of magnetic adatom-induced Majorana vortex and its hybridization with field-induced Majorana vortex in an iron-based superconductor, *Nat. Commun.* **12**, 1348 (2021).
- [9] D. Wang, J. Wiebe, R. Zhong, G. Gu, and R. Wiesendanger, Spin-Polarized Yu-Shiba-Rusinov States in an Iron-Based Superconductor, *Phys. Rev. Lett.* **126**, 076802 (2021).
- [10] D. Chatzopoulos, D. Cho, K. M. Bastiaans, G. O. Stefansen, D. Bouwmeester, A. Akbari, G. Gu, J. Paaske, B. M. Andersen and M. P. Allan, Spatially dispersing Yu-Shiba-Rusinov states in the unconventional superconductor FeTe_{0.55}Se_{0.45}, *Nat. Commun.* **12**, 298 (2021).
- [11] See the Supplemental Material At xxx for details about the DFT calculations, the self-consistent solutions of the BdG equations in lattice model, the proof for the equivalence between vortex case and impurity case, and the solutions for the majorana zero modes.
- [12] V. Thampy, J. Kang, J. A. Rodriguez-Rivera, W. Bao, A. T. Savici, J. Hu, T. J. Liu, B. Qian, D. Fobes, Z. Q. Mao, C. B. Fu, W. C. Chen, Q. Ye, R. W. Erwin, T. R. Gentile, Z. Tesanovic, and C. Broholm, Friedel-Like Oscillations from Interstitial Iron in Superconducting Fe_{1+y}Te_{0.62}Se_{0.38}, *Phys. Rev. Lett.* **108**, 107002 (2012).
- [13] N. Hao and J. Hu, Topological Phases in the Single-Layer FeSe. *Phys. Rev. X* **4**, 031053 (2014).
- [14] Z. Wang, P. Zhang, G. Xu, L. K. Zeng, H. Miao, X. Xu, T. Qian, H. Weng, P. Richard, A. V. Fedorov, H. Ding, X. Dai, and Z. Fang, Topological nature of the FeSe_{0.5}Te_{0.5} superconductor. *Phys. Rev. B* **92**, 115119 (2015).
- [15] X. Wu, S. Qin, Y. Liang, H. Fan, and J. Hu, Topological characters in Fe(Te_{1-x}Se_x) thin films. *Phys. Rev. B* **93**, 115129 (2016).
- [16] G. Xu, B. Lian, P. Tang, X.-L. Qi, and S.-C. Zhang, Topological Superconductivity on the Surface of Fe-Based Superconductors. *Phys. Rev. Lett.* **117**, 047001 (2016).
- [17] N. Hao and J. Hu, Topological quantum states of matter in iron-based superconductors: from concept to material realization. *Natl. Sci. Rev.* **6**, 213 (2019).
- [18] D. Wang, L. Kong, P. Fan, H. Chen, S. Zhu, W. Liu, L. Cao, Y. Sun, S. Du, J. Schneeloch, R. Zhong, G. Gu, L. Fu, H. Ding, H.-J. Gao, *Science*, **362**, 333-335 (2018).
- [19] K. Jiang, X. Dai, and Z. Wang, Quantum Anomalous Vortex and Majorana Zero Mode in Iron-Based Superconductor Fe(Te,Se), *Phys. Rev. X* **9**, 011033 (2019).
- [20] X. Wu, S. B. Chung, C. Liu, E. Kim, *Phys. Rev. Research* **3**, 013066 (2021).
- [21] C. Chiu and Z. Wang, *Phys. Rev. Lett.* **128**, 237001 (2022).
- [22] Z. Zhou and J. Klinovaja, arXiv:2109.08200 (2021).
- [23] M. E. Flatté and J. M. Byers, Local Electronic Structure of a Single Magnetic Impurity in a Superconductor, *Phys. Rev. Lett.* **78**, 3761 (1997).
- [24] R. K ummel, Electronic Structure of Superconductors with Dilute Magnetic Impurities, *Phys. Rev. B.* **6**, 2617 (1972).
- [25] A. Yazdani, B. A. Jones, C. P. Lutz, M. F. Crommie, and D. M. Eigler, Probing the Local Effects of Magnetic Impurities on Superconductivity, *Science*, **275** (5307) (1997).
- [26] M. I. Salkola, A. V. Balatsky, and J. R. Schrieffer, Spectral properties of quasiparticle excitations induced by magnetic moments in superconductors, *Phys. Rev. B* **55**, 12648 (1997).
- [27] T. Meng, J. Klinovaja, S. Hoffman, P. Simon, and D. Loss, Superconducting gap renormalization around two magnetic impurities: From Shiba to Andreev bound states, *Phys. Rev. B* **92**, 064503 (2015).

- [28] L. Fu and C. L. Kane, Superconducting Proximity Effect and Majorana Fermions at the Surface of a Topological Insulator, *Phys. Rev. Lett.* **100**, 096407 (2008).
- [29] R. Song, P. Zhang and N. Hao, Phase-Manipulation-Induced Majorana Mode and Braiding Realization in Iron-Based Superconductor Fe(Te,Se), *Phys. Rev. Lett.* **128**, 016402 (2022).
- [30] Wen-Yu Shan, Jie Lu, Hai-Zhou Lu, and Shun-Qing Shen, Vacancy-induced bound states in topological insulators, *Phys. Rev. B* **84**, 035307 (2011).
- [31] Xiao-Liang Qi, Taylor L. Hughes, S. Raghu, and Shou-Cheng Zhang, Time-Reversal-Invariant Topological Superconductors and Superfluids in Two and Three Dimensions *Phys. Rev. Lett.* **102**, 187001 (2009).
- [32] J. R. Colbert and P. A. Lee, Proposal to measure the quasiparticle poisoning time of Majorana bound states, *Phys. Rev. B* **89**, 140505(R) (2014).
- [33] Fan Zhang, C. L. Kane, and E. J. Mele, Time-Reversal-Invariant Topological Superconductivity and Majorana Kramers Pairs, *Phys. Rev. Lett.* **111**, 056402 (2013).
- [34] S. S. Zhang, J.-X. Yin, G. Dai, L. Zhao, T.-R. Chang, N. Shumiya, K. Jiang, H. Zheng, G. Bian, D. Multer, M. Litskevich, G. Chang, I. Belopolski, T. A. Cochran, X. Wu, D. Wu, J. Luo, G. Chen, H. Lin, F.-C. Chou, X. Wang, C. Jin, R. Sankar, Z. Wang, and M. Z. Hasan, *Phys. Rev. B* **101**, 100507(R) (2020).
- [35] P. Zhang, K. Yaji, T. Hashimoto, Y. Ota, T. Kondo, K. Okazaki, Z. Wang, J. Wen, G. D. Gu, H. Ding, and S. Shin, *Science* **360**, 182 (2018).
- [36] T. Choi, W. Paul, S. Rolf-Pissarczyk, A. J. Macdonald, F. D. Natterer, K. Yang, P. Willke, C. P. Lutz, and A. J. Heinrich, Atomic-scale sensing of the magnetic dipolar field from single atoms, *Nat. Nanotechnol.* **12**, 420 (2017).
- [37] T.g Choi, C. P. Lutz, A. J. Heinrich, Studies of magnetic dipolar interaction between individual atoms using ESR-STM, *Current Applied Physics*, **17**, 11, (2017).

DFT CALCULATING METHODS

First-principles calculations were performed by density functional theory (DFT) using the Vienna ab initio simulation package (VASP) [1, 2]. The plane-wave basis with an energy cutoff of 350 eV was adopted. The electron-ion interactions were modeled by the projector augmented wave potential (PAW) [3] and the exchange-correlation functional was approximated by the Perdew-Burke-Ernzerhof-type (PBE) generalized gradient approximation (GGA) [4]. Here we use the parameter "I-CONSTRAINED-M" in VASP to constrain the direction of the Fe impurity always along the z axis and give the substrate a very weak magnetic background. As shown in Fig. 5, the differential charge density can reflect the coupling between the impurity and substrate, as the height increases, the chemical adsorption will turn into physical adsorption. To estimate the value of $J(r, z)$, we can set the impurity having a FM and AFM coupling with its nearest iron atoms respectively. And using a simple Heisenberg Hamiltonian, we can calculate the strength of exchange coupling. The local Hamiltonian reads

$$H_M = -J_H \sum_{NN} S_{imp} \cdot S_{NN}, \quad (6)$$

where S_{imp} and S_{NN} is the magnetic moment of the impurity and its nearest neighbor iron atoms. Because the impurity has four nearest neighbor, we can get

$$\Delta E = H_{AFM} - H_{FM} = 8J_H S_{imp} S_{NN}. \quad (7)$$

The effective magnetic field generated by the impurity is

$$h_{imp} = \frac{n \langle S_{imp} \rangle}{\mu_B} \int J_H(r) dr \quad (8)$$

where n , S_{imp, μ_B} labels the concentration of localized moments, the average value of the localized spins, Bohr magneton and ferromagnetic exchange integral, respectively [5]. For a single impurity, we have $n = 1$ and $J_H(r) = J_H \delta(r)$. The coupling Hamiltonian is

$$H_{coup} = \int dr J(\mathbf{r}, z_0) \mathbf{S}_{imp} \cdot \sigma \quad (9)$$

The exchange interaction is very local, so we can assume that $J(\mathbf{r}, z_0) = J \delta(r)$, and then we can adopt a mean-field approximation as

$$H_{coup} = \langle J S_{imp} \rangle \sum_{\sigma} \sigma c_{i_0}^{\dagger} c_{i_0}. \quad (10)$$

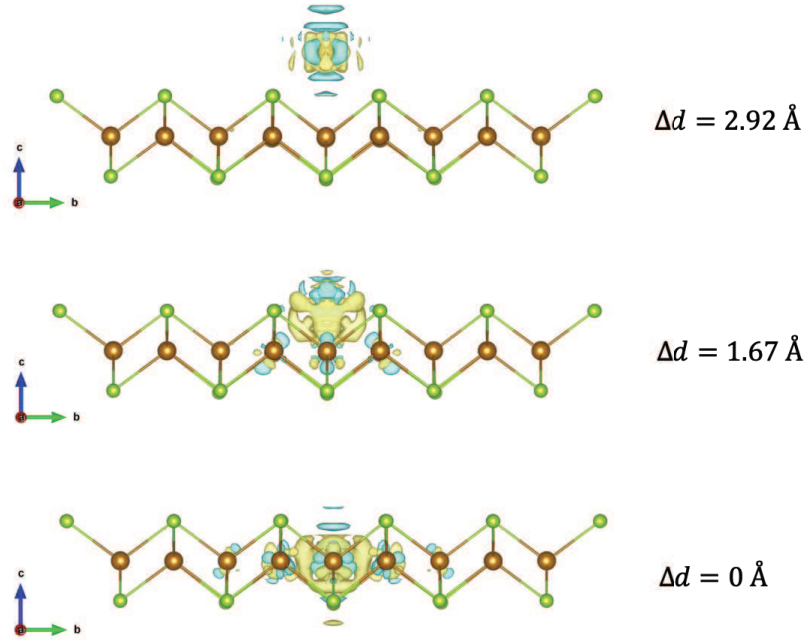


FIG. 5: Differential charge density of different height (a) 2.92Å, (b) 1.67Å and (c) 0Å.

Comparing Eq. 10 and Eq. 8, we find that the existence of the magnetic impurity is equivalent to applying a local magnetic field at the impurity site. So the strength of the exchange coupling can be characterized by the effective magnetic field generated by the impurity, which can be calculated as

$$\langle JS_{imp} \rangle = \frac{\Delta E}{8S_{NN}} \quad (11)$$

In our calculations, the S_{NN} is set to be $0.05\mu_B$, $S_{imp} = \pm 3\mu_B$ for FM and AFM coupling respectively.

BDG METHOD IN LATTICE MODEL

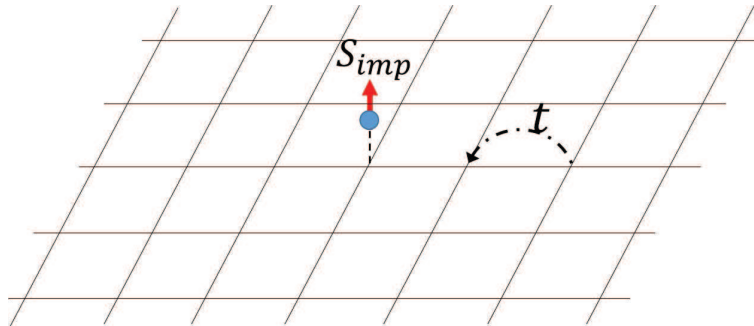


FIG. 6: Scheme of the lattice model.

To model the superconductivity in right way, it is better to start from the experimental measurements. From Fig. 3 in the experimental paper[6], one can find that the two YSR states always cross at a critical value of coupling

between the impurity and substrate. Note that applying magnetic field is equivalent to change the coupling between the impurity and substrate and just move the crossing point. This robust crossing feature is crucial to decide how to model the superconductivity in right way. There are two possibilities to model the superconductivity related to the STM/STS experiments. i.e., the topological surface Dirac bands plus trivial s-wave pairing and trivial bulk multi-bands plus S_{\pm} pairing. In the former one, the superconductivity of the surface Dirac bands is from the self-proximity effect or inter-band scattering around $\bar{\Gamma}$ point in the surface Brillouin zone. The trivial bulk bands around \bar{M} point have no effect to the surface Dirac bands near $\bar{\Gamma}$ point. Thus, the superconductivity of the surface Dirac bands near $\bar{\Gamma}$ point can be reduced to have the trivial s-wave pairing, if the surface Dirac bands play a dominated role. We calculate the impurity induced YSR states for both models to see which one is consistent with the experimental measurements.

Topological surface Dirac model with trivial s-wave pairing

We consider a square lattice, the topological surface Dirac Hamiltonian can be expressed as

$$H_{surf} = - \sum_i \mu c_i^\dagger c_i - it \sum_{\langle i,j \rangle} c_{i\sigma}^\dagger (\mathbf{S}^{\sigma\sigma'} \times \hat{\mathbf{d}}_{ij}) \cdot \hat{\mathbf{z}} c_{j\sigma'} \quad (12)$$

which includes the on-site term, and linear Dirac term. Now a magnetic impurity is put onto the site i_0 and thus would introduce an exchange term as

$$H_{coup} = -J(c_{i_0\uparrow}^\dagger c_{i_0\uparrow} - c_{i_0\downarrow}^\dagger c_{i_0\downarrow}), \quad (13)$$

which performs like an effective magnetic field generated by the impurity. Note that S_{imp} is merged into J for simplicity. And when superconductivity is induced, the surface trivial s-wave Cooper pairing potential is introduced as

$$H_{\Delta} = \sum_i (\Delta c_{i\uparrow}^\dagger c_{i\downarrow}^\dagger + h.c.). \quad (14)$$

The total Hamiltonian is

$$H = H_{surf} + H_{coup} + H_{\Delta}. \quad (15)$$

We can perform the Bogoliubov transformation

$$c_{i\sigma} = \sum_n' (u_{i\sigma}^n \gamma_n - \sigma v_{i\sigma}^{n*} \gamma_n^\dagger) \quad (16)$$

where $'$ denotes summation over the positive eigenvalues, and numerically solve the equations

$$\sum_j \hat{H}_{ij} \phi_j = E_n \phi_i \quad (17)$$

in the Nambu spinor representation $\phi_i = (u_{i\uparrow}^n, u_{i\downarrow}^n, v_{i\uparrow}^n, v_{i\downarrow}^n)^T$ [7]. The matrix elements read

$$\hat{H}_{ij} = \begin{pmatrix} \Lambda_{ij\uparrow} & T_{ij}^{\uparrow\downarrow} & 0 & \Delta_i \\ T_{ij}^{\downarrow\uparrow} & \Lambda_{ij\downarrow} & \Delta_i & 0 \\ 0 & \Delta_i & -(\Lambda_{ij\uparrow})^* & (T_{ij}^{\uparrow\downarrow})^* \\ \Delta_i & 0 & (T_{ij}^{\downarrow\uparrow})^* & -(\Lambda_{ij\downarrow})^* \end{pmatrix}, \quad (18)$$

where $\Lambda_{ij\sigma} = -(\mu + \sigma J \delta_{ii_0}) \delta_{ij}$. $T_{ij}^{\sigma\sigma'} = -it(\mathbf{S}^{\sigma\sigma'} \times \hat{\mathbf{d}}_{ij}) \cdot \hat{\mathbf{z}}$. And the order parameter Δ_i should be self-consistently determined as

$$\Delta_i(T) = \frac{g}{2} \sum_n' (u_{i\uparrow}^n v_{i\downarrow}^{n*} + u_{i\downarrow}^n v_{i\uparrow}^{n*}) \tanh\left(\frac{E_n}{k_B T}\right) \quad (19)$$

To get the numerical results, we have adopted a 25×25 lattice. The hopping parameter $t = 10 \text{ meV}$, homogeneous order parameter $\Delta_0 = 2 \text{ meV}$ and chemical potential $\mu = 0.1t$. The calculated spectrum of H in Eq. 15 is shown in Fig. 7 (a) and (b), from which, one can find there exist a robust level crossing for two YSR states against the external magnetic field. The level crossing is schematically shown in Fig. 7 (d). The existence of level crossing is consistent with the experimental measurements, and indicates a QPT happens. At the QPT, the order parameter at the impurity site is discontinuous and suddenly change sign as shown in Fig. 7 (c).

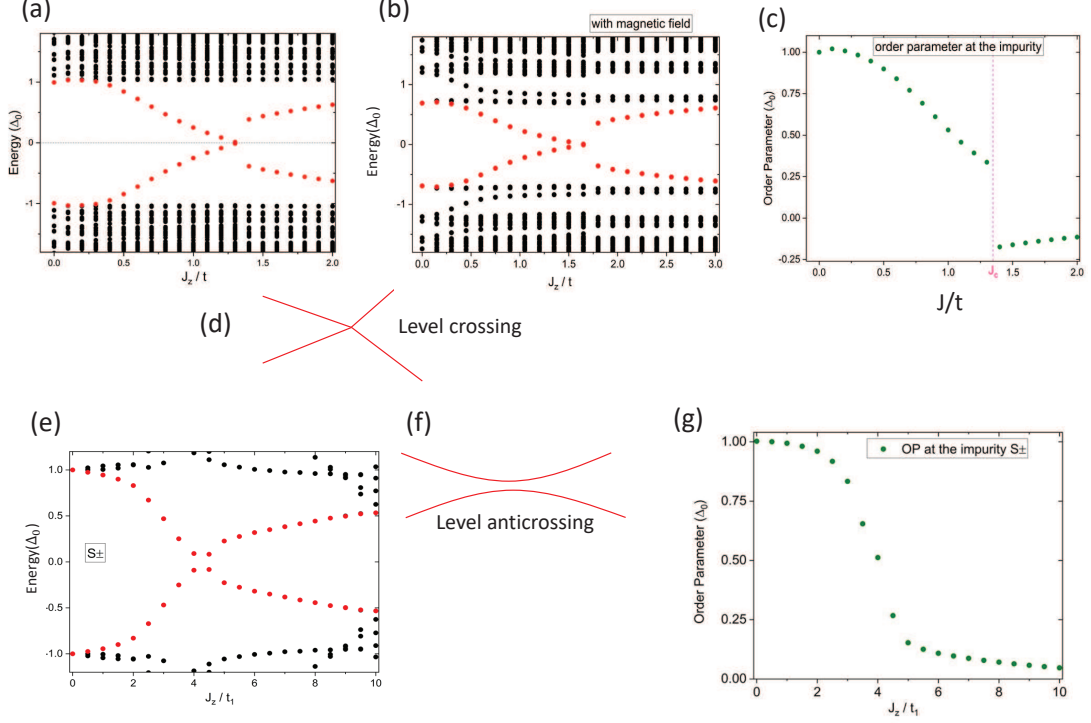


FIG. 7: (a)-(c) The energy spectrum and superconducting order parameter of topological surface Dirac superconducting state with magnetic impurity scattering described by Hamiltonian H in Eq. 15. (a) without magnetic field and (b) with magnetic field. In (c), the superconducting order parameter at the impurity site as a function of J . (d) The scheme of level crossing. (e)-(g) The energy spectrum and superconducting order parameter of two-band model with S_{\pm} pairing and magnetic impurity scattering described by Hamiltonian H' in Eq. 20. (e) without magnetic field. (f) The scheme of level anticrossing. (g) the superconducting order parameter at the impurity site as a function of J .

Trivial bulk Multi-bands model with S_{\pm} pairing

Now we will check the same process between the magnetic impurity and bulk state of iron-based superconductor. The main difference is the pairing pattern. The numerical calculation is also carried on a square lattice and the minimal two-orbital band structure is adopt[8]. The two-orbitals model is described by

$$H_b = \sum_k \psi_k^\dagger [(\epsilon_+(k) - \mu) + \epsilon_-(k)\tau_z + \epsilon_{xy}(k)\tau_x] \psi_k,$$

with $\psi_k^\dagger = [d_{xz}^\dagger(k), d_{yz}^\dagger(k)]$, and

$$\begin{aligned} \epsilon_{\pm}(k) &= \frac{\epsilon_x(k) \pm \epsilon_y(k)}{2} \\ \epsilon_x(k) &= -2t_1 \cos k_x - 2t_2 \cos k_y - 4t_3 \cos k_x \cos k_y \\ \epsilon_y(k) &= -2t_2 \cos k_x - 2t_1 \cos k_y - 4t_3 \cos k_x \cos k_y \\ \epsilon_{xy}(k) &= -4t_4 \sin k_x \sin k_y \end{aligned}$$

After introducing the interacting term and at the mean field approximation, we obtain the BdG Hamiltonian as

$$H_b + H'_\Delta = - \sum_{ij,\alpha\beta} (t_{ij,\alpha\beta} + \mu\delta_{ij}\delta_{\alpha\beta})d_{i\alpha}^\dagger d_{j\beta} + \sum_{\langle\langle i,j \rangle\rangle} (\Delta_{ij,\alpha\beta}d_{i\alpha\uparrow}^\dagger d_{j\beta\downarrow}^\dagger + h.c.).$$

Here, $\Delta_{ij,\alpha\beta}$ describes the next-nearest neighbor pairing with S_\pm symmetry *i.e.*, $\cos k_x \cos k_y$ form in momentum space. The IFI induced intra-orbital scattering is considered as

$$H'_{coup} = J \sum_{\alpha} (d_{i_0\alpha\uparrow}^\dagger d_{i_0\alpha\uparrow} - d_{i_0\alpha\downarrow}^\dagger d_{i_0\alpha\downarrow}).$$

The total Hamiltonian is

$$H' = H_b + H'_\Delta + H'_{coup} \quad (20)$$

The self-consistent condition is

$$\Delta_{ij}(T) = \frac{g}{2} \sum'_{\langle\langle i,j \rangle\rangle n} (u_{i\uparrow}^n v_{j\downarrow}^{n*} + u_{i\downarrow}^n v_{j\uparrow}^{n*}) \tanh\left(\frac{E_n}{k_B T}\right),$$

and the final homogeneous order parameter is expressed as $\bar{\Delta}_i = \frac{1}{8} \sum_{j,\alpha\beta} \Delta_{ij}^{\alpha/\beta}$. The calculated spectrum of H' in Eq. 20 is shown in Fig. 7 (e), from which, one can find there only exist a level anticrossing for two YSR states. The level anticrossing is schematically shown in Fig. 7 (f). This feature is inconsistent with the experimental measurements, and no QPT happens. The order parameter at the impurity site continuously decays to zero as J change, as shown in Fig. 7 (g).

By comparing the calculation results of the above two models with the experimental measurements[6], we arrive the right model related with the STS experiments is the topological surface Dirac model with trivial s-wave pairing. We start with this model in the main text.

THE EQUIVALENCE BETWEEN VORTEX CASE AND IMPURITY CASE

Numerical proof for the antiperiodic boundary condition for the impurity case

We first calculate the spectrum of the geometries, as shown in Fig. 8(a), (c) and (e) with periodic boundary condition *i.e.* $\psi(r, \theta) = \psi(r, \theta + 2\pi)$. The numerical results are shown in Fig. 8(b), (d) and (e), respectively. All π -phase disk and 0-phase ring and 0 – π disk junction have no in-gap bound states. The numerical result for the 0 – π disk junction is not consistent with the well-know 0 – π line junction results. Therefore, the periodic boundary condition is not right for the 0 – π disk junction, and the *antiperiodic boundary condition* *i.e.* $\psi(r, \theta) = -\psi(r, \theta + 2\pi)$ has to be used for the 0 – π junction disk in impurity case.

Vortex case

For comparison, we also analyzed the general vortex-induced Majorana mode. When there exist quantum vortices, the SC order parameter should have a attached phase as $\Delta = \Delta(r)e^{i\theta}$. The complete Hamiltonian can be expressed as

$$\begin{pmatrix} -\mu & -e^{-i\theta}v_F(\partial_r - \frac{i}{r}\partial_\theta) & \Delta(r)e^{i\theta} & 0 \\ e^{i\theta}v_F(\partial_r + \frac{i}{r}\partial_\theta) & -\mu & 0 & \Delta(r)e^{i\theta} \\ \Delta(r)e^{-i\theta} & 0 & \mu & e^{-i\theta}v_F(\partial_r - \frac{i}{r}\partial_\theta) \\ 0 & \Delta(r)e^{-i\theta} & -e^{i\theta}v_F(\partial_r + \frac{i}{r}\partial_\theta) & \mu \end{pmatrix} \quad (21)$$

Correspondingly, the trivial wave functions should have this form

$$\psi(r, \theta) = e^{i\theta} \begin{pmatrix} u_\uparrow(r) \\ e^{i\theta}u_\downarrow(r) \\ e^{-i\theta}v_\downarrow(r) \\ v_\uparrow(r) \end{pmatrix} \quad (22)$$

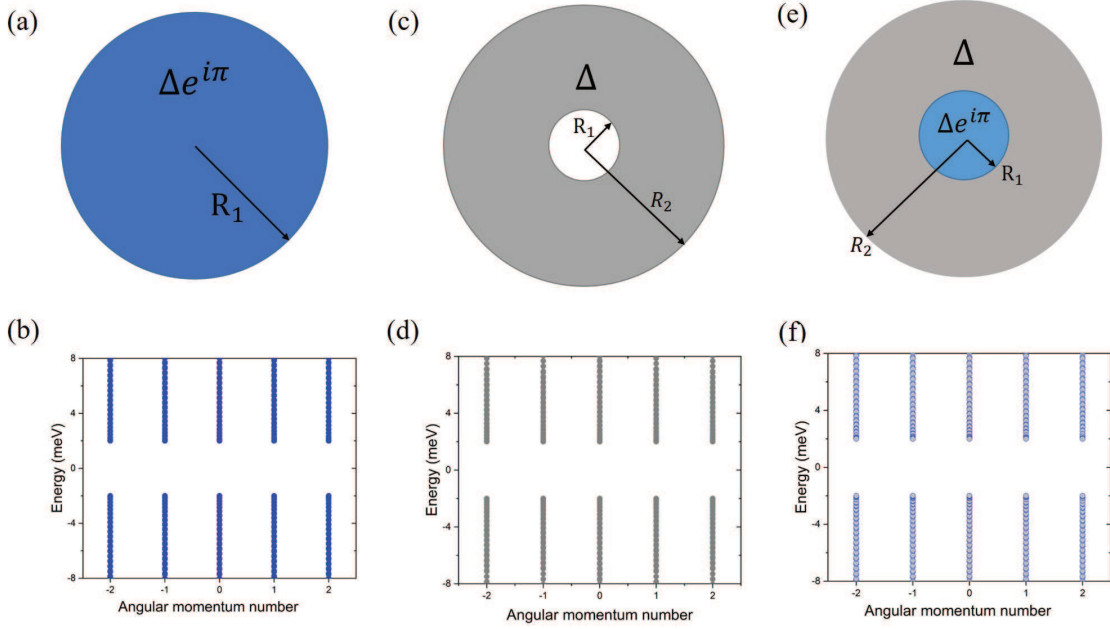


FIG. 8: Schematic diagram of (a) A π -phase disk and (c) A 0-phase ring, (e) A combo of (a) and (b). (b), (d) and (e) The energy spectrum with a periodic boundary condition for (a), (c) and (e), respectively.

Also, the Majorana condition requests that

$$l = 0 \quad (23)$$

$$u_{\uparrow}(r) = -\eta v_{\uparrow}(r) \quad (24)$$

$$u_{\downarrow}(r) = \eta v_{\downarrow}(r) \quad (25)$$

The radial equation can be obtained as

$$\begin{pmatrix} -\mu & -v_F(\partial_r + \frac{l+1}{r}) & \Delta(r) & 0 \\ v_F(\partial_r - \frac{l}{r}) & -\mu & 0 & \Delta(r) \\ \Delta(r) & 0 & \mu & v_F(\partial_r + \frac{l}{r}) \\ 0 & \Delta(r) & -v_F(\partial_r - \frac{l-1}{r}) & \mu \end{pmatrix} \begin{pmatrix} u_{\uparrow}(r) \\ u_{\downarrow}(r) \\ v_{\downarrow}(r) \\ v_{\uparrow}(r) \end{pmatrix} = E \begin{pmatrix} u_{\uparrow}(r) \\ u_{\downarrow}(r) \\ v_{\downarrow}(r) \\ v_{\uparrow}(r) \end{pmatrix} \quad (26)$$

Here, we first derive the analytic solution for Majorana mode when $\Delta(r)$ is approximated as a constant Δ_0 . Similarly, the equation can be simplified as

$$u_{\uparrow}''(r) + \left(\frac{2}{\xi_0} + \frac{1}{r}\right)u_{\uparrow}'(r) + \left(\frac{1}{\xi_0^2} + \frac{1}{r\xi_0} + k_F^2\right)u_{\uparrow}(r) = 0 \quad (27)$$

the solution can be obtained as :

$$u_{\uparrow}(r) = c_1 J_0(k_F r) e^{-r/\xi_0} \quad (28)$$

$$u_{\downarrow}(r) = -c_1 J_1(k_F r) e^{-r/\xi_0}, \quad (29)$$

which is consistent with Ref. [9, 10].

Now we will perform the numerical solution of Eq. (26), the method is the same as above. The space variation of order parameter is adopted as $\Delta(r) = \Delta_0 \tanh \frac{r}{\xi_0}$. The results are shown in Fig. 10. For the vortex condition, its Hamiltonian can be expressed as

$$H_{\nu} = [v_F(k_x \sigma_y - k_y \sigma_x) - \mu] \tau_z + \Delta_0 e^{i\nu\theta} \tau_{+} + \Delta_0 e^{-i\nu\theta} \tau_{-}, \quad (30)$$

where $\nu = \pm 1$ for (anti-) vortex, $\tau_{\pm} = \tau_x \pm i\tau_y$. The wave functions of a vortex has a form shown in Eq. (22), we

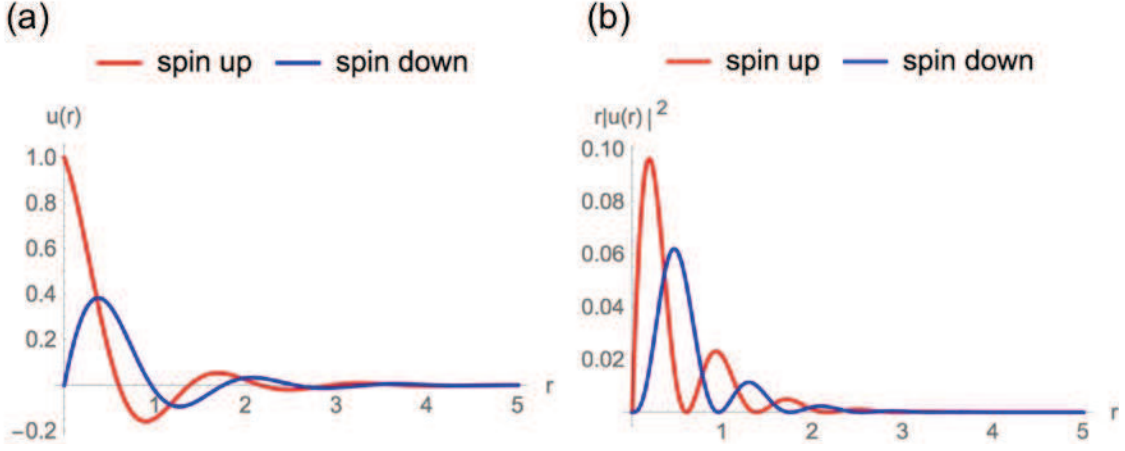


FIG. 9: (a) wave functions and (b) the probability density for the vortex-induced Majorana mode.

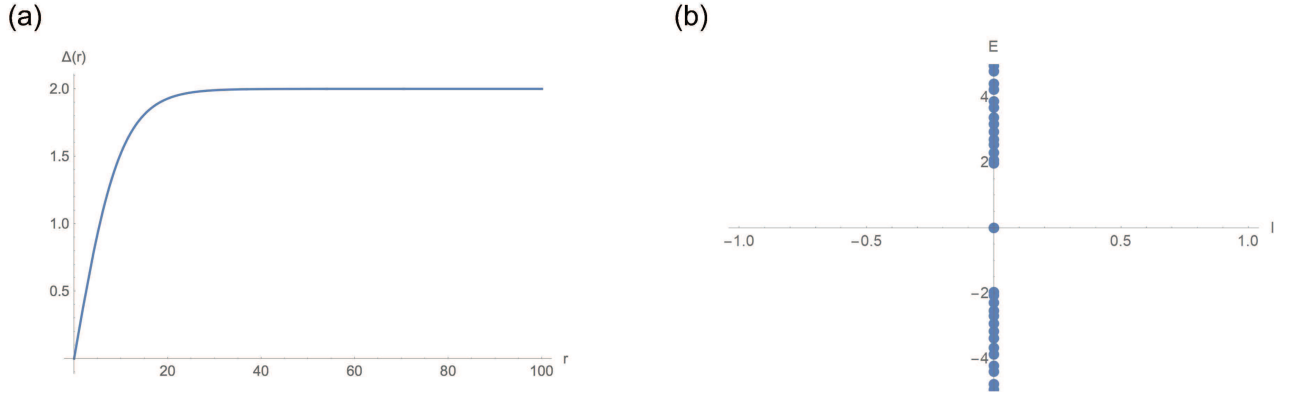


FIG. 10: (a) The order parameter from the core to the edge of a vortex and (b) the energy spectrum of momentum $l = 0$.

name it ψ_{v+} . And the wave function of an anti-vortex can be easily obtained as

$$\psi_{v-} = e^{il\theta} \begin{pmatrix} e^{-i\theta} u_{\uparrow}(r) \\ u_{\downarrow}(r) \\ v_{\downarrow}(r) \\ e^{i\theta} v_{\uparrow}(r) \end{pmatrix}. \quad (31)$$

Both ψ_{v+} and ψ_{v-} are periodic. However we can apply this gauge transformation

$$\psi'_{v\pm} = U_{\pm} \psi_{v\pm}, \quad (32)$$

here $U_{+} = \text{diag}(e^{-i\theta/2}, e^{-i\theta/2}, e^{i\theta/2}, e^{i\theta/2})$ and $U_{-} = U_{+}^*$. It is obvious that the new wave functions $\psi'_{v\pm}$ is anti-periodic, the corresponding Hamiltonian can be obtained as $H'_{v\pm} = U_{\pm} H_{\nu} U_{\pm}^{-1}$, which reads

$$H'_{v+} = H'_{v-} = [v_F(k_x \sigma_y - k_y \sigma_x) - \mu] \tau_z + \Delta_0 \tau_x. \quad (33)$$

Eq. (33) has the same form with Eq. (34) when $B = 0$. So its proved that the bound state in our $0 - \pi$ disk junction is equivalent to the vortex condition, the difference is that in our $0 - \pi$ disk junction model the time-reversal symmetry is preserved so that the Majorana mode is a helical mode instead of a chiral mode. That can also be reflected by the numerical calculated results.

SOLUTION OF MAJORANA ZERO MODE

Analytic solution

The Hamiltonian of a magnetic field applied to a superconductor with a Dirac-type topological surface state can be expressed as $H = \int d^2r \Psi^\dagger(r) \mathcal{H} \Psi(r)$, where

$$\mathcal{H} = [v_F(k_x \sigma_y - k_y \sigma_x) - \mu] \tau_z + \alpha \boldsymbol{\sigma} \cdot \mathbf{B} + \Delta(r) \tau_x. \quad (34)$$

Here $\Psi = (c_\uparrow, c_\downarrow, c_\downarrow^\dagger, -c_\uparrow^\dagger)$ denotes the Nambu basis, σ_i and τ_i ($i = x, y, z$) are Pauli matrices but spans spin and Nambu space respectively, $\Delta(r)$ takes the real value due to no superconducting vortex. $\mathbf{B}(\mathbf{r})$ is the external magnetic field $\mathbf{B} = (B_x, B_y, B_z)$. Due to the existence of impurity, translation invariance is broken. Thus we need to solve Eq. (1) in real space with cylindrical coordinate system, and we have following transformation:

$$\begin{aligned} k_x - ik_y &= -ie^{-i\theta} \partial_r - \frac{e^{-i\theta}}{r} \partial_\theta \\ k_x + ik_y &= -ie^{i\theta} \partial_r + \frac{e^{i\theta}}{r} \partial_\theta \end{aligned}$$

Substituting it into Eq. (1), we get the complete form BdG Hamiltonian as

$$\begin{pmatrix} \alpha B_z - \mu & -e^{-i\theta} v_F (\partial_r - \frac{i}{r} \partial_\theta) & \Delta(r) & 0 \\ e^{i\theta} v_F (\partial_r + \frac{i}{r} \partial_\theta) & -\alpha B_z - \mu & 0 & \Delta(r) \\ \Delta(r) & 0 & \alpha B_z + \mu & e^{-i\theta} v_F (\partial_r - \frac{i}{r} \partial_\theta) \\ 0 & \Delta(r) & -e^{i\theta} v_F (\partial_r + \frac{i}{r} \partial_\theta) & -\alpha B_z + \mu \end{pmatrix}. \quad (35)$$

Here, we assume the magnetic field is along the z direction. The BdG equation is

$$\mathcal{H} \psi(r, \theta) = E \psi(r, \theta). \quad (36)$$

Assuming the trivial wave function with the *antiperiodic boundary condition* has the form

$$\psi(r, \theta) = e^{il\theta} \begin{pmatrix} e^{-i\theta/2} u_\uparrow(r) \\ e^{i\theta/2} u_\downarrow(r) \\ e^{-i\theta/2} v_\downarrow(r) \\ -e^{i\theta/2} v_\uparrow(r) \end{pmatrix} \quad (37)$$

Then we can obtain the radial equation of Eq. (36) as:

$$(\alpha B_z - \mu) u_\uparrow(r) - v_F (\partial_r + \frac{l + \frac{1}{2}}{r}) u_\downarrow(r) + \Delta(r) v_\downarrow(r) = E u_\uparrow(r) \quad (38)$$

$$v_F (\partial_r - \frac{l - \frac{1}{2}}{r}) u_\uparrow(r) - [\alpha B_z + \mu] u_\downarrow(r) - \Delta(r) v_\uparrow(r) = E u_\downarrow(r) \quad (39)$$

$$\Delta(r) u_\uparrow(r) + (\alpha B_z + \mu) v_\downarrow(r) - v_F (\partial_r + \frac{l + \frac{1}{2}}{r}) v_\uparrow(r) = E v_\downarrow(r) \quad (40)$$

$$\Delta(r) u_\downarrow(r) - v_F (\partial_r - \frac{l - \frac{1}{2}}{r}) v_\downarrow(r) + (\alpha B_z - \mu) v_\uparrow(r) = -E v_\uparrow(r) \quad (41)$$

The matrix form is :

$$\begin{pmatrix} \alpha B_z - \mu & -v_F (\partial_r + \frac{\nu+1}{r}) & \Delta(r) & 0 \\ v_F (\partial_r - \frac{\nu}{r}) & -\alpha B_z - \mu & 0 & \Delta(r) \\ \Delta(r) & 0 & \alpha B_z + \mu & v_F (\partial_r + \frac{\nu+1}{r}) \\ 0 & \Delta(r) & -v_F (\partial_r - \frac{\nu}{r}) & -\alpha B_z + \mu \end{pmatrix}, \quad (42)$$

where $\nu = l - \frac{1}{2}$. The Majorana solution requests $\mathcal{C}\psi(r, \theta) = \eta\psi(r, \theta)$, where the particle-hole operator $\mathcal{C} = \tau_y\sigma_y K$, with K the complex conjugation operator, and η is some constant. Without loss of generality, we assume $u_{\uparrow(\downarrow)}(r)$ and $v_{\uparrow(\downarrow)}(r)$ is real. This yields the following constraint condition:

$$u_{\uparrow}(r) = \eta v_{\uparrow}(r) \quad (43)$$

$$u_{\downarrow}(r) = \eta v_{\downarrow}(r) \quad (44)$$

$$l = 0 \quad (45)$$

Obviously, η can only be $+1$ or -1 , and they correspond to the exponential increase and decay solution, respectively. For an infinite large 2D space, only $\eta = -1$ is reasonable. And then the equation set of Eq. (38)-(41) can be reduced as

$$(\alpha B_z - \mu)u_{\uparrow}(r) - \left[v_F(\partial_r + \frac{1}{2r}) + \Delta(r) \right] u_{\downarrow}(r) = E u_{\uparrow}(r), \quad (46)$$

$$\left[v_F(\partial_r + \frac{1}{2r}) + \Delta(r) \right] u_{\uparrow}(r) - [\alpha B_z + \mu] u_{\downarrow}(r) = E u_{\downarrow}(r), \quad (47)$$

For the Majorana condition, we can set $E = 0$.

Now, let's check the simplest condition where $B_z = 0$, which means there is no magnetic effect and then the system should return to the TI+SC model, however with a antiperiodic boundary condition. When $B_z = 0$, Eq. (12) and (13) can be reduced to :

$$u''_{\uparrow(\downarrow)}(r) + \frac{u'_{\uparrow(\downarrow)}(r)}{r} + \left(\frac{\mu^2 + \Delta_0^2}{v_F^2} - \frac{1}{4r^2} \right) u_{\uparrow(\downarrow)}(r) + \frac{2\Delta_0}{v_F} \left[u'_{\uparrow(\downarrow)}(r) + \frac{1}{2r} u_{\uparrow(\downarrow)}(r) \right] = 0 \quad (48)$$

The solution of $u_{\uparrow}(r)$ is

$$u_{\uparrow}(r) = c_1 \frac{e^{-ik_F r}}{\sqrt{r}} e^{-r/\xi_0} + c_2 \frac{e^{ik_F r}}{\sqrt{r}} e^{-r/\xi_0} \quad (49)$$

$$u_{\downarrow}(r) = -i(c_1 \frac{e^{-ik_F r}}{\sqrt{r}} - c_2 \frac{e^{ik_F r}}{\sqrt{r}}) e^{-r/\xi_0} \quad (50)$$

where $\xi_0 = \frac{v_F}{\xi_0}$, $k_F = \frac{\mu}{v_F}$. Note that c_1 should equal to c_2 to ensure $u(r)$ is real, and then the radial wave functions can be reduced as $u_{\uparrow/\downarrow}(r) \propto J_{\mp 1/2}(k_F r) e^{-r/\xi_0}$, by contrast with the vortex condition the order of Bessel function has a $\frac{1}{2}$ shift. Note that we have obtain one zero energy mode solution as shown in Eqs. 37, 49 and 50. However, the Hamiltonian in Eq. 34 has the time-reversal symmetry (TRS) when $B_z = 0$. Therefore, there must exist another zero-energy mode, which is the TRS partner of the first one denoted by Eqs. 37, 49 and 50. Both of them form the Kramers degenerate states. The TRS operator takes the form $\mathcal{T} = i\tau_0\sigma_y K$.

When the magnetic field $\mathbf{B} = (B_x, B_y, B_z)$ is taken into account, the Hamiltonian for the zero modes in Eq. 42 can be expressed as

$$H_{zero} = (-i\sigma_y \hat{T}(r) + \alpha B_x \sigma_x + \alpha B_y \sigma_y + \alpha B_z \sigma_z) \tau_z + \Delta(r) \tau_x \quad (51)$$

Here, $\hat{T}(r) = v_F(\partial_r + \frac{1}{2r})$. In such a case, one can define a mirror symmetry $\mathcal{M}_{l=0} = i\sigma_y \tau_y \hat{O}(r)$. $\hat{O}(r)$ is a spacial inverse operator along the radial direction with the inverse center at R_0 . Note that $\hat{T}(r)$ and $\Delta(r)$ changes sign under the operation $\hat{O}(r)$. Now, one can get $[\mathcal{M}_{l=0}, H_{zero}] = 0$ for non-zero B_x and B_z . For non-zero B_y , $[\mathcal{M}_{l=0}, H_{zero}] \neq 0$. Therefore, a pair of zero modes are robust against non-zero B_x and B_z , but are fragile for non-zero B_y . When $B_z \neq 0$, we set $m_z = \alpha B_z$, the Zeeman term has the form of $m_z \tau_0 \sigma_z$, and the splitting between two zero energy modes can be estimated by

$$\langle \psi_1(r, \theta) | m_z \tau_0 \sigma_z | \psi_2(r, \theta) \rangle = 0 \quad (52)$$

Therefore, the z -direction Zeeman coupling cannot split the zero-energy mode. However, if we directly solve the Eq. 46 and 47 with $B_z \neq 0$, one can find that only parameter k_F is modified as $k_F = \frac{\sqrt{\mu^2 - m_z^2}}{v_F}$. It is easy to find that if $|m_z| > |\mu|$ the wave function is divergent when $r \rightarrow \infty$. Actually, only when $\mu > m_z$ it's topological nontrivial.

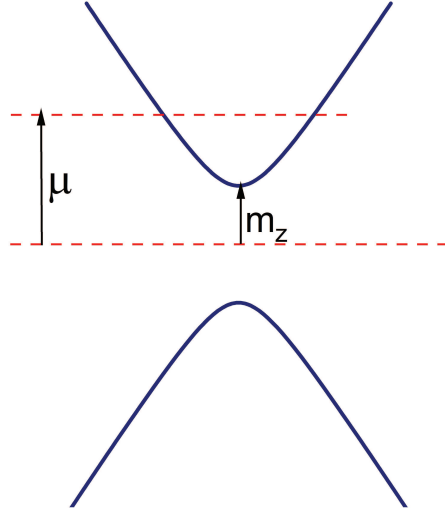


FIG. 11: TI with a z-direction magnetic field. Only when $\mu > m_z$ there exists a spin-momentum-locked fermi surface and it is topological nontrivial.

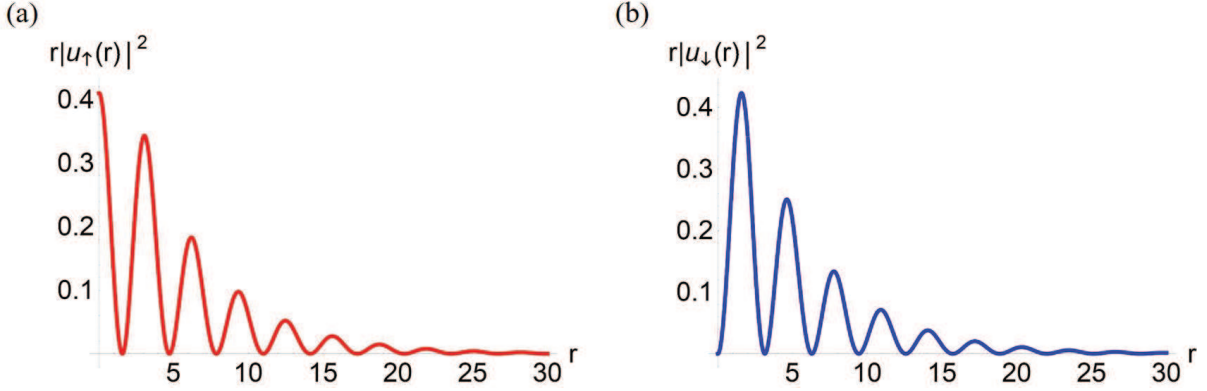


FIG. 12: Wave functions of analytic solution.

Quasiparticle's scattering

From Eq. (49) and (50), it's easy to find that the wave functions of Majorana modes can always be divided into two parts according to its radial propagating directions, i.e. towards or dorsad the impurity center. We define $e^{-ik_F r}$ as a converging wave. Here the scattering effect caused by the impurity should be considered. In a 2D space where the rotation symmetry is preserved, the scattering wave function should be described by the cylindrical wave. The scattering process can be understood as Fig. 13, we name the wave functions of incoming and scattering as ψ_{in} and ψ_s , respectively, their specific form is :

$$\psi_{in} = C \frac{e^{-ik_F r}}{\sqrt{r}} e^{r/\xi_0} \quad (r < R_0) \quad (53)$$

$$\psi_s = f(\theta) \frac{e^{ikr}}{\sqrt{r}}, \quad (54)$$

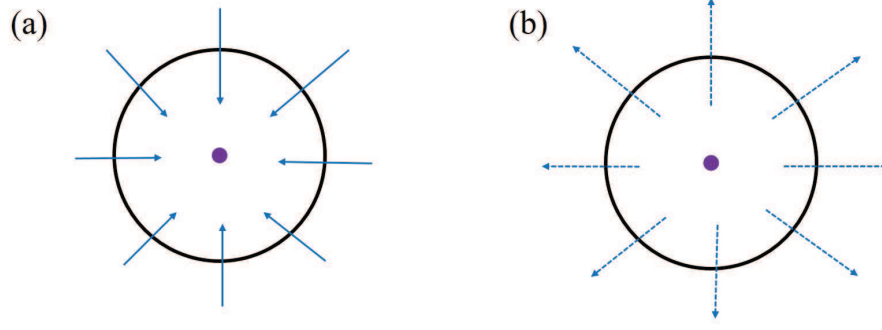


FIG. 13: (a) The converging cylindrical wave propagates to the impurity and (b) is scattered into a diverging cylindrical wave.

where $f(\theta)$ is the scattering amplitude, and the scattering interface is defined as $\sigma(\theta) = |f(\theta)|^2$ [11]. The incoming and scattering current density can be defined by the following formula

$$j = \frac{i\hbar}{2m}(\psi\nabla\psi^* - \psi^*\nabla\psi). \quad (55)$$

So the specific expression of the scattering wave function should be solved from the flow conservation and Schrödinger equation :

$$j_{in} = j_s \quad (56)$$

$$\frac{\hbar^2}{2m}\nabla^2\psi_s + U(r)\psi_s = E\psi_s \quad (57)$$

where $U(r)$ is the scattering potential, for a single impurity we can consider it as a local potential $U(r) = U_0\delta(r)$, and the elastic scattering requests $E = 0$ since the scattered particle is Majorana fermion. According to the method of partial, we can decompose the scattering wave function into different angular-momentum channel by using

$$e^{ikr\cos\theta} = J_0(kr) + \sum_{n=1}^{\infty} i^n J_n(kr) \cos n\theta \quad (58)$$

It is known that for a local δ potential, only s wave i.e. $l = 0$ is involved, so it's obvious to simplify the scattering wave function as $\psi_s(r, \theta) = f(\theta)J_0(kr)/\sqrt{r}$. Thus the additional density of states (DOS) at zero energy caused by the elastic scattering is

$$N_s(E = 0, r, \theta) \propto r|\psi_s(r, \theta)|^2 \propto J_0^2(kr). \quad (59)$$

Here $|f(\theta)|$ is approximated to a constant because $\int_0^{2\pi} f(\theta)d\theta = constant$. Considering this modulation about zero-energy DOS, we obtain

$$N(E = 0, r) = N_s^0 J_0^2(kr) + N_M^0(r) \quad (60)$$

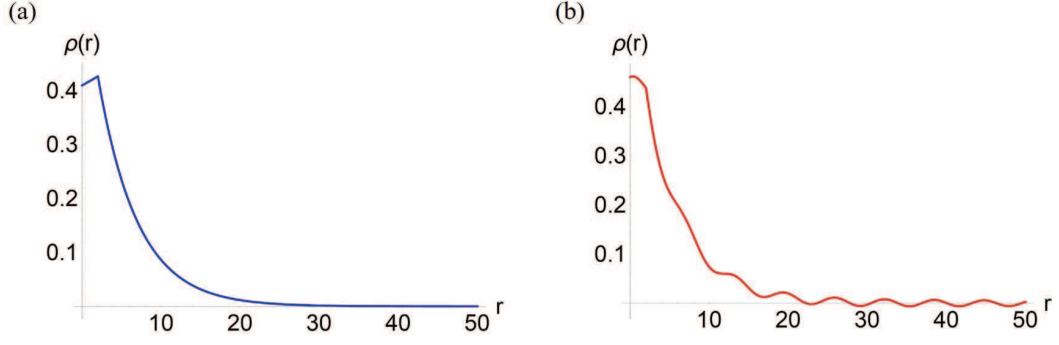


FIG. 14: Probability density (a) before and (b) after taking into account of the quasiparticle-scattering effect, the former is a simple summation of spin-up and spin-down part in Fig. 12 and the latter include the scattering wave functions.

Numerical Solution

Now we use Bessel functions as a complete orthogonal base to expand the wave function [12]. That is

$$u_{\uparrow}(r) = \sum_{n=1}^N u_n^{\uparrow} \varphi_{\nu,n}(r) \quad (61)$$

$$u_{\downarrow}(r) = \sum_{n=1}^N u_n^{\downarrow} \varphi_{\nu+1,n}(r) \quad (62)$$

$$v_{\downarrow}(r) = \sum_{n=1}^N v_n^{\downarrow} \varphi_{\nu+1,n}(r) \quad (63)$$

$$v_{\uparrow}(r) = \sum_{n=1}^N v_n^{\uparrow} \varphi_{\nu,n}(r) \quad (64)$$

where $\nu = l - \frac{1}{2}$, $\varphi_{\nu,n} = \frac{\sqrt{2}}{R J_{\nu+1}(j_{\nu,n} \frac{r}{R})} J_{\nu}(j_{\nu,n} \frac{r}{R})$, N is the cutoff number. Then the radial equation Eq. 42 can be reduced as a $4N \times 4N$ matrix and the its eigenvalues are the energies. We define:

$$T_{ij}^{\nu} = \alpha \int_0^R B_z \varphi_{\nu,i}(r) \varphi_{\nu,j}(r) r dr \quad (65)$$

$$V_{ij}^{\nu,\nu+1} = v_F \int_0^R r \varphi_{\nu,i}(r) (\partial_r + \frac{\nu+1}{r}) \varphi_{\nu+1,j}(r) dr \quad (66)$$

$$S_{ij}^{\nu+1,\nu} = v_F \int_0^R r \varphi_{\nu+1,i}(r) (\partial_r - \frac{\nu}{r}) \varphi_{\nu,j}(r) dr \quad (67)$$

$$\Delta_{ij}^{\nu} = \int_0^R \Delta(r) \varphi_{\nu,i}(r) \varphi_{\nu,j}(r) r dr \quad (68)$$

Here, the order parameter varies in the space can be approximately calculated as $\Delta(r) = \Delta_0 (1 - \alpha \frac{1 - \cos(2k_F r)}{k_F^2 r^2})$. Then the eigenvalue equation can be expressed as :

$$\text{Det} \begin{pmatrix} T^{\nu} - \mu & -V^{\nu,\nu+1} & \Delta^{\nu} & 0 \\ S^{\nu+1,\nu} & -T^{\nu+1} - \mu & 0 & \Delta^{\nu+1} \\ \Delta^{\nu} & 0 & T^{\nu} + \mu & V^{\nu+1,\nu} \\ 0 & \Delta^{\nu+1} & -S^{\nu,\nu+1} & -T^{\nu+1} + \mu \end{pmatrix} = E \quad (69)$$

To get the numerical results, we have set the radius of the disk as $R = 800 \text{ \AA}$, the Fermi velocity $v_F = 200 \text{ meV \AA}$ as the experimental measurement [13], $\mu = 1 \text{ meV}$ and the cut-off number $N = 50$ which is accurate enough to affirm the Majorana zero-energy mode. The results are shown in Fig. 15.

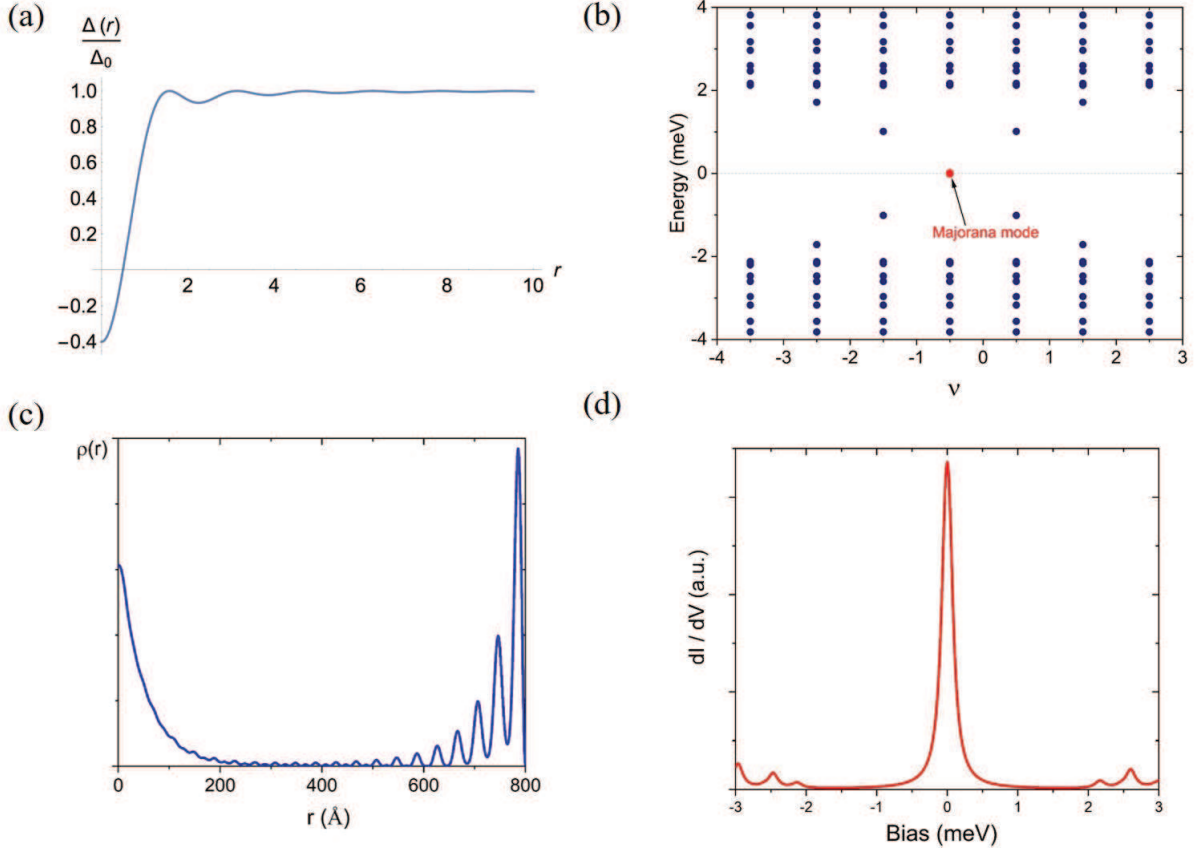


FIG. 15: (a) Variation of order parameter in space; (b) Energy spectrum for $\nu = -\frac{1}{2}$ ($l = 0$); (c) Radial probability density; (d) Simulated STM spectrum at the core $r = 0$.

The Majorana condition requests that $\mathcal{C}\psi = \eta\psi$, in the main text we choose $\eta = -1$ because we adopt a infinite large diameter of the disk and if $\eta = 1$ the wave functions have an exponentially increasing form, which is not physical. However if the diameter is finite, $\eta = 1$ would be reasonable and forms another probability-density peak at the boundary. Thus the zero-energy solution should be a linear combination of $\eta = \pm 1$ as

$$\psi = \sum_{\eta} a_{\eta} \varphi_{\eta}. \quad (70)$$

And that is the reason why every zero-energy mode contains both the core and edge state.

In the line-type $0 - \pi$ junction, the gapless bound state has energy dispersion as $E = \pm v_F k_y$. When the line is bent to form a ring, the energy becomes discrete and can be estimated by the Bohr-Sommerfeld quantized condition, which is :

$$E_n = \pm v_F k_n \quad (71)$$

$$k_n 2\pi R_0 = 2n\pi \quad (n = 0, 1, 2, \dots) \quad (72)$$

Thus the mini gap is $\Delta E = v_F/R_0$. With a large Fermi velocity and a small radius of the π -phase area, the bound states except zero-energy Majorana mode are hidden in the ground state.

* Electronic address: zhangping@iapcm.ac.cn

† Electronic address: haon@hmfl.ac.cn

[1] G. Kresse and J. Furthmüller, Phys. Rev. B **54**, 11169 (1996).

- [2] G. Kresse and D. Joubert, Phys. Rev. B **59**, 1758 (1999).
 - [3] P. E. Blchl, Phys. Rev. B **50**, 17953 (1994).
 - [4] J. P. Perdew, K. Burke, and M. Ernzerhof, Phys. Rev. Lett. **77**, 3865 (1996).
 - [5] A. I. Buzdin, Rev. Mod. Phys. **77**, 935 (2005).
 - [6] P. Fan et al., Nat. Commun. **12**, 1348 (2021)
 - [7] Jian-Xin Zhu, Wonkee Kim, C. S. Ting, and J. P. Carbotte, Quasiparticle States around a Nonmagnetic Impurity in a d-Density-Wave State of High- T_c Cuprates, Phys. Rev. Lett. **87**, 197001 (2001).
 - [8] S. Raghu et al., PRB, **77**, 220503(R) (2008)
 - [9] Takuto Kawakami and Xiao Hu, Evolution of Density of States and a Spin-Resolved Checkerboard-Type Pattern Associated with the Majorana Bound State. Phys. Rev. Lett. **115**.177001 (2015).
 - [10] Hao-Hua Sun, Kai-Wen Zhang, et al, Majorana Zero Mode Detected with Spin Selective Andreev Reflection in the Vortex of a Topological Superconductor. Phys. Rev. Lett. **116**.257003 (2016).
 - [11] Sakurai J J, Advanced Quantum Mechanics[M], Addison Wesley, New York, (1967).
 - [12] Li Mao and Chuanwei Zhang, Robustness of Majorana modes and minigaps in a spin-orbit-coupled semiconductor-superconductor heterostructure, Phys. Rev. B **82**, 174506 (2010).
 - [13] D.Wang, L. Kong, P. Fan, H. Chen, S. Zhu, W. Liu, L. Cao, Y. Sun, S. Du, J. Schneeloch, R. Zhong, G. Gu, L. Fu, H. Ding, and H.-J. Gao, Evidence for Majorana bound states in an iron-based superconductor, Science **362**, 333 (2018).
-